Published in final edited form as:
Dev Cell. 2011 October 18; 21(4): 708–721. doi:10.1016/j.devcel.2011.08.019.

The tetraspanin CD63 regulates ESCRT-independent and dependent endosomal sorting during melanogenesis

Guillaume van Niel[1,2], **Stéphanie Charrin**[4,*], **Sabrina Simoes**[1,2,*], **Maryse Romao**[1,2,3], **Leila Rochin**[1,2], **Paul Saftig**[5], **Michael S. Marks**[6], **Eric Rubinstein**[4], and **Graça Raposo**[1,2,3]

[1]Institut Curie, Centre de Recherche, F-75248 Paris, France

[2]Unité Mixte de Recherche 144, Centre National de la Recherche Scientifique, F-75248 Paris, France

[3]Cell and Tissu Imaging facility (IBiSA), Institut Curie, F-75248 Paris, France

[4]Inserm U602, Hôpital Paul Brousse, Villejuif 94800, France

[5]Biochemisches Institut, Christian Albrechts Universität Kiel, Germany

[6]Departments of Pathology and Laboratory Medicine and Physiology, University of Pennsylvania, Philadelphia, Pennsylvania 19104, USA

Summary

Cargo sorting to intraluminal vesicles (ILVs) of multivesicular endosomes is required for numerous physiological processes including lysosome-related organelle (LRO) biogenesis. PMEL – a component of melanocyte LROs (melanosomes) – is sorted to ILVs in an ESCRT-independent manner, where it is proteolytically processed and assembled into functional amyloid fibrils during melanosome maturation. Here we show that the tetraspanin CD63 directly participates in ESCRT-independent sorting of the PMEL luminal domain, but not of traditional ESCRT-dependent cargoes, to ILVs. Inactivating CD63 in cell culture or in mice impairs amyloidogenesis and downstream melanosome morphogenesis. Whereas CD63 is required for normal PMEL luminal domain sorting, the disposal of the remaining PMEL transmembrane fragment requires functional ESCRTs but not CD63. In the absence of CD63, the PMEL luminal domain follows this fragment and is targeted for ESCRT-dependent degradation. Our data thus reveal a tight interplay regulated by CD63 between two distinct endosomal ILV sorting processes for a single cargo during LRO biogenesis.

Introduction

Sorting of integral membrane protein cargoes to the intraluminal vesicles (ILVs) of multivesicular endosomes (MVEs) is a key step in many physiological processes including cessation of growth factor signaling, lysosomal degradation, exosome secretion, lysosome related organelle (LRO) biogenesis, and perhaps even amyloid formation (Raiborg and Stenmark, 2009; Raposo et al., 2007; Simons and Raposo, 2009; van Niel et al., 2006). Lysosomal degradation generally requires the recognition of ubiquitinated protein cargoes by components of the Endosomal Sorting Complex Required for Transport (ESCRT)

Corresponding authors: Guillaume van Niel, guillaume.van-niel@curie.fr, Phone: +33 156246442. Graça Raposo, Graca.Raposo@curie.fr, Phone: +33 156246441.

*Both authors contributed equally to this work

Competing financial interests
The authors declare no competing financial interests.

machinery (Gruenberg and Stenmark, 2004; Hurley, 2008), in which the ESCRT-0, -I and -II complexes recognize and sequester ubiquitinated proteins in the endosomal membrane and the ESCRT-III complex effects membrane budding and scission. However, sorting of some proteins within MVEs, including physiologically critical cargoes of exosomes and LRO biogenesis intermediates, occurs independently of ubiquitination or ESCRT components (Buschow et al., 2009; Simons and Raposo, 2009; Theos et al., 2006b; Trajkovic et al., 2008). The mechanisms underlying ESCRT-independent ILV sorting and their temporal and spatial relationship with ESCRT-dependent sorting processes remain poorly understood.

ESCRT-independent ILV sorting is important to generate precursors for melanosomes. Melanosomes are LROs of melanocytes and other pigment cells that are specialized for melanin pigment synthesis. Melanosomes co-exist with lysosomes and form through four morphologically distinct stages (Seiji et al., 1963a), the earliest of which (stage I and II premelanosomes) lack pigment but harbor fibrils that assemble into fibrillar sheets upon which newly synthesized melanins polymerize during melanosome maturation. The fibrils underlie the elongated shape of melanosomes and are composed largely of proteolytic lumenal fragments of the amyloidogenic pigment cell-specific type I integral membrane protein, PMEL. The fibrils, which are thought to concentrate melanins and to prevent the accumulation of toxic intermediates generated during pigment synthesis (reviewed in (Raposo et al., 2007; Theos et al., 2005; Watt et al., 2009), form in association with the ILVs of stage I premelanosomes (Hurbain et al., 2008) upon which PMEL accumulates (Raposo et al., 2001). Stage I premelanosomes are vacuolar MVE intermediates that are accessed by endocytic tracers after 15 min, contain few (n=2–6) ILV profiles, and harbor abundant clathrin-containing bilayered coats at their limiting membrane (Raposo et al., 2001) that are enriched in the ESCRT-0 component Hrs (Theos et al., 2006b). Paradoxically, PMEL is sorted to ILVs by an ESCRT-independent mechanism (Theos et al., 2006b; Truschel et al., 2009). The molecular basis for this sorting event is not known, but it requires a lumenal subdomain of PMEL and does not require any cytoplasmic domain determinant or ubiquitination (Theos et al., 2006b). Sorting to ILVs correlates with proteolytic processing steps that release the fibrillogenic luminal domain from the transmembrane form of PMEL to initiate amyloid formation (Berson et al., 2001; Berson et al., 2003; Fowler et al., 2006; Kummer et al., 2009). These processing events also generate transmembrane fragments of PMEL that are destined for gamma-secretase-dependent degradation by as yet incompletely defined mechanisms (Kummer et al., 2009).

In other cell systems, ESCRT-independent formation of ILVs in MVEs requires lipid rafts and ceramide (de Gassart et al., 2003; Trajkovic et al., 2008) and/or protein aggregation (Fang et al., 2007; Vidal et al., 1997). Other proposed regulators of ILV formation are proteins of the tetraspanin family (TSPAN) (Charrin et al., 2009), which are selectively enriched in the ILVs of MVEs and in exosomes derived from them (Simons and Raposo, 2009; van Niel et al., 2006). Among TSPAN, CD63 is particularly enriched intracellularly; in most cells it localizes predominantly to late endosomes and lysosomes (Pols and Klumperman, 2009), whereas in specialized cells CD63 is also present in LROs such as endothelial cell Weibel Palade Bodies, platelet dense granules and neutrophil myeloperoxidase granules (Pols and Klumperman, 2009; Raposo and Marks, 2007). Here, we investigated the role of CD63 in PMEL sorting to ILVs and its ability to generate amyloid fibrils *in vitro* and *in vivo*. We show that CD63 functions in ESCRT-independent ILV formation, and that it thereby modulates the fate of two distinct domains of PMEL that are destined for amyloidogenesis and degradation. Importantly our data reveal a tightly regulated interplay between ESCRT-independent and dependent sorting of distinct functional domains of the same proteolytically cleaved cargo protein to regulate organelle biogenesis.

Results

CD63 localizes to melanosomes and to PMEL-positive MVEs

We first tested whether CD63 localizes to melanosomal compartments in pigmented MNT-1 melanoma cells, a faithful model for eumelanogenesis (Raposo et al., 2001). Immunofluorescence microscopy (IFM) analysis revealed that CD63 (Fig. 1a), but not the related tetraspanin CD81 **(Suppl. Fig. S1a)**, localizes to a subset of premelanosomes as shown by its partial co-localization with PMEL labeled by antibody HMB50. By immunoelectron microscopy (IEM) using immunogold labeling on ultrathin cryosections, CD63 localizes broadly to multiple intracellular compartments, including predominantly mature melanosomes (stages I–IV; Fig. 1b **left panel,** c), but only 5 to 10% localized to lysosomes (Fig. 1c) as supported by the low degree of overlap with LAMP-1 by IFM (**Suppl. Fig. S1b**). Consistent with the degree of overlap by IFM, quantification of the immunogold labeling shows that 20–25% of CD63 is detected on PMEL-positive MVEs (Fig. 1b, c). Within MVEs, more than 75% of the labeling for both CD63 and PMEL is detected on ILVs rather than the limiting membrane (Fig. 1b, d). This indicates that CD63, like PMEL, is preferentially sorted to ILVs within melanocyte MVEs.

Our previous studies revealed that PMEL sorting to ILVs does not require ubiquitination or functional ESCRT components (Theos et al., 2006b; Truschel et al., 2009). Consistently, both CD63 and PMEL were detected in MVEs in ultrathin cryosections of MNT-1 cells in which the ESCRT-I subunit, Tsg101, was depleted by siRNA treatment (**Suppl. Fig. S1c, d**). These observations agree with previous findings that CD63-positive MVEs continue to form despite concomitant inactivation of subunits from four different ESCRT complexes (Stuffers et al., 2009), and suggest that both CD63 and PMEL undergo ESCRT-independent sorting into the ILVs of MVEs.

CD63 is required for intraluminal vesicle formation and PMEL distribution

We next explored the potential requirement for CD63 in ESCRT-independent sorting of PMEL in MVEs by analyzing MNT-1 cells in which CD63 was depleted by siRNA treatment. By western blot analysis, treatment with either of two CD63-specific siRNAs decreased the expression of CD63 by more than 80% (Fig. 2a). As in untreated cells, (Hurbain et al., 2008; Raposo et al., 2001), MNT-1 cells treated with control siRNA and analyzed by conventional electron microscopy (EM) harbour coated MVEs containing an average of 5 ILV profiles (Fig. 2b*left*, d). By IEM, the ILVs are enriched in PMEL (Fig. 2c*left*, e). In CD63-inactivated cells, whereas vacuolar endosomes with characteristic bilayered coats (Fig. 2b, arrows) are unusually abundant (see Fig. 3d and f), they are largely depleted of ILVs, with an average of less than 2 ILV profiles per endosome (Fig. 2b*right*, d). Concomitantly, whereas labeling for PMEL was still detected in coated endosomes in CD63-inactivated cells, it was mostly localized to the limiting membrane (Fig. 2c *right*), resulting in more than a 2-fold reduction in the fraction of PMEL present on ILVs (Fig. 2e). On those ILVs that were detectable in CD63-depleted cells, the level of labeling for PMEL was similar to that observed on ILVs in control cells (Fig. 2f) suggesting that the main effect of CD63 depletion was on ILV formation at the coated endosome rather than on Pmel17 sorting to the ILVs.

CD63 is required for the generation of PMEL-driven fibrils and premelanosomes *in vitro* and *in vivo*

PMEL amyloid fibrils have been proposed to nucleate on ILVs in the MVE lumen (Berson et al., 2001; Hurbain et al., 2008; Theos et al., 2006b). We therefore evaluated the requirement for CD63 in the formation of PMEL amyloid fibrils. The antibody HMB45 detects an epitope on Golgi-modified PMEL that is most enriched on proteolytic fragments

that accumulate on fibrils (Harper et al., 2008; Hoashi et al., 2006; Kushimoto et al., 2001). Inactivation of CD63, but not of CD81 (**Suppl. Fig. S2a, b**), resulted in a consistent and specific reduction (93% +/− 7% compared to control) in HMB45 labeling by both immunoblotting of fibril-enriched detergent-insoluble cell fractions (Fig. 3a) and by IFM (Fig. 3b). Nevertheless, CD63-depleted MNT-1 cells retained punctate labeling by IFM for PMEL using antibody HMB50, which recognizes a wider panel of PMEL forms (Harper et al., 2008) (Fig. 3c). These data suggest that CD63 is not required for PMEL expression or trafficking to post-Golgi structures but is required for downstream fibril formation.

To further investigate the requirement for CD63 in melanogenesis, we analyzed the morphology of melanosomal compartments in CD63-inactivated cells by EM. MNT-1 cells treated with control siRNA display numerous stage II premelanosomes harboring organized fibrils (Fig. 3d **left, arrowheads,** and 3e1). CD63 depletion is accompanied by a dramatic and quantitative reduction in the number of stage II premelanosomes containing fully formed amyloid sheets (Fig. 3d **right,** 3f). As a potential consequence of inhibiting fibrillogenesis after 3 days of CD63 depletion, the number of stage III pigmented melanosomes also decreased, while pigmented round melanosomal structures with unstructured melanin deposits accumulated (Fig. 3d **right, arrowheads,** 3f). Consistent with this accumulation and with the lack of effect of reduced PMEL expression on melanogenesis (Theos et al., 2006a), melanin content slightly increased and melanin synthesizing enzymes localized appropriately to the aberrant melanosomes in CD63-depleted cells (**Suppl. Fig. S3a, b**). Moreover, relative to controls, CD63-depleted cells harbored 4-fold the number of compartments with lysosomal morphology (round compartments of 500 nm diameter containing few internal vesicles, dense material and lamellar structures) and additional unique organelles with clearly visible dense aggregates (Fig. 3e2, 3e3), similar to those observed in cells with impaired fibril formation due to a loss of PMEL processing (Berson et al., 2003). This suggested that as a consequence of impaired delivery of PMEL to ILVs of coated MVES in the absence of CD63, amyloidogenesis and consequent melanosome maturation are disrupted.

To investigate whether CD63 depletion affects melanogenesis in a physiological setting, we analyzed pigment cells in $CD63^{-/-}$ mice (Schroder et al., 2009). Compared to $CD63^{+/+}$ mice, $CD63^{-/-}$ mice display variable graying of coat colour (not shown). Because of potential compensatory effects observed in skin melanocytes of mice with melanogenesis defects (Lopes et al., 2007), we analyzed melanosome morphology in retinal pigment epithelium (RPE) in which the compensatory effect is less apparent. By EM, RPE of CD63−/− mice have a dramatic reduction in melanosome number (Fig. 3g). Compared to the characteristic ellipsoidal shaped melanosomes in the RPE of control mice (Fig. 3g, top), the remaining melanized melanosomes in CD63−/− RPE are round (Fig. 3g, *bottom*). The round shape is consistent with a defect in the formation of the structural scaffold formed by PMEL-derived amyloid fibers in PMEL mutant *silver* mice (Theos et al., 2006a). These observations indicate that amyloidogenesis and consequent melanosome maturation are impaired in the absence of CD63 *in vivo*.

CD63 is required for amyloidogenic processing of PMEL

PMEL sorting to ILVs correlates with proteolytic processing steps that are required for PMEL to transition to the amyloid form (Berson et al., 2003; Theos et al., 2006b). These steps include: a) cleavage of full-length PMEL by a prohormone convertase into an amyloidogenic lumenal Mα fragment and a disulfide-linked transmembrane domain-containing Mβ fragment (Berson et al., 2001); b) further processing of Mβ by a site 2 protease (S2P) to release Mα from the membrane and to produce a C Terminal Fragment (CTF) that is degraded by gamma-secretase (Kummer et al., 2009); and c) further processing of Mα by unknown proteases to smaller fragments found in mature fibers (Kushimoto et al.,

2001; Watt et al., 2009) (Fig 4a). To test whether CD63 depletion affects PMEL processing, we assayed siRNA-treated MNT-1 cells by western blotting using an antibody to the PMEL cytosolic domain (αPmel-C). In control cells, this antibody detects the immature core-glycosylated PMEL P1 form (90 kDa), the Mβ (28 kDa) product of PC cleavage, and CTF (10kD) (Figs. 4a, b). In CD63-depleted cells (Fig. 2a), Mβ and CTF bands are detectable but modestly decreased in intensity (Fig. 4b). To distinguish whether this reflects decreased production or accelerated degradation of Mβ and CTF, we blocked degradation of CTF (but of not Mβ or P1) by treating cells with the gamma-secretase inhibitor, DAPT (**Suppl. Fig. S4)**. Treatment of either control or CD63-depleted cells with DAPT induced a similar level of accumulated CTF (Fig. 4c). This suggested CD63 depletion accelerates CTF degradation but does not affect upstream PMEL cleavages.

To further dissect how CD63 depletion affects PMEL processing and fibril maturation, we probed immunoblots of cell fractions with antibodies to additional PMEL epitopes. Mα fragments that are released from the membrane anchor by PC and S2P cleavage assemble into Triton X-100 insoluble fibrils (Berson et al., 2003), detected by antibody αPmel-N to the PMEL N-terminus, and then matured by further processing to smaller digestion products detected by antibodies HMB45 and I51 (Harper et al., 2008; Hoashi et al., 2006; Watt et al., 2009). In TX-100-insoluble fractions of CD63 siRNA-treated cells, αPmel-N reactive Mα (but not αPmel-C-reactive cytoplasmic fragments of PMEL) accumulated at normal or higher levels relative to control cells (Fig. 4d and e), but smaller HMB45- and I51-reactive fragments were depleted (Figs. 3a, 4f). These data confirm that CD63 is not required for PC and S2P processing and release of the PMEL fibrillogenic lumenal domain, but indicate that CD63 is required either for further processing subsequent to ILV sorting or for stabilization of the resultant fragments.

CD63 interacts with the PMEL CTF

To test whether CD63 might influence PMEL ILV partitioning and processing directly, we assayed for physical interactions between CD63 and PMEL. To this end we first expressed PMEL in HeLa cells by transfection and used co-immunoprecipitation from cell lysates prepared in mild detergent (Brij 97) to preserve tetraspanin-partner interactions. At steady state, PMEL CTF was coimmunoprecipitated with anti-CD63 but not with anti-CD81 (Fig. 5a **upper right**; note the signal above the background bands, detected in untransfected HeLa cells, **upper left**). Similar co-immunoprecipitation assays with endogenous PMEL in MNT-1 cells failed to detect an interaction (not shown). However, consistent with the shorter half-life of PMEL and its CTF in melanocytic cells compared with transfected HeLa cells (Berson et al., 2001), CTF was co-immunoprecipitated with CD63 - but not with the related tetraspanins CD81 or CD9 – after treatment of MNT-1 cells with DAPT (Fig. 5b **top panels**). Conversely, CD63 but not CD81 could be co-immunoprecipitated with αPmel-C from DAPT-treated MNT-1 cell lysates (Fig. 5b, **bottom panels**). MART-1, a known partner of PMEL (Hoashi et al., 2005), also interacted with both PMEL CTF and CD63 (Fig. 5b), but was not necessary for the interaction between PMEL and CD63 as indicated by co-immunoprecipitation assays from HeLa cells which lack MART-1 (Fig. 5a). Together, these data indicate that CD63 interacts with the CTF, likely reflecting a transient CTF-dependent interaction with PMEL prior to cleavage by S2P.

The C-Terminal fragment of PMEL is degraded in an ESCRT-I –dependent manner

Unlike the PMEL-lumenal domain which is clearly associated with ILVs of stage I melanosomes (*e.g.* Fig. 2c), the cytoplasmic domain is mainly detected on the limiting membrane at steady state (Berson et al., 2003; Raposo et al., 2001), suggesting a distinct fate for the CTF after release from the lumenal domain. Given that αPmel-C labeling is localized within clathrin and Hrs- positive regions {Raposo, 2001 #568;Theos, 2006 #465} and that

accelerated degradation (Fig. 4b) in absence of CD63 is correlated to an increased number of lysosomal structures (Fig. 3f), we tested whether CTF disposal requires ESCRT-dependent endosomal sorting by following the fate of the CTF in MNT-1 cells depleted for Tsg101 (Fig. 6a). Like the ubiquitinated substrate MART-1 (Truschel et al., 2009), the CTF, but not other PMEL isoforms, accumulated in lysates from Tsg101-depleted cells relative to controls (Fig. 6a). By IFM, labeling for the Pmel C-terminus in control cells yields largely diffuse tubular or small punctate labeling representing the ER, and perinuclear labeling representing largely the Golgi (Fig. 6b **upper panels** and Fig. 6c, **left panels**; see also (Harper et al., 2008)). By contrast, labeling for CTF in Tsg101-depleted cells was detected in enlarged vacuoles that surrounded structures labeled for the luminal domain of PMEL (Fig 6b **lower panels**). IEM analysis revealed that the PMEL lumenal domain was largely associated with small ILVs whereas the PMEL cytoplasmic domain accumulated mostly at the limiting membrane (**Suppl. Fig. S5a, b**). These observations suggest that while sorting of the PMEL luminal domain occurs in an ESCRT-independent manner, the CTF degradation requires ESCRT-I function and is initiated from MVEs.

To infer the intracellular site of CTF degradation in MNT-1 cells, we allowed CTF to accumulate by inhibiting gamma-secretase with DAPT. By IFM analysis, the largely tubulovesicular ER labeling for the PMEL C-terminus observed in control cells was replaced in DAPT-treated cells by vesicular structures that remained distinct from those harboring the PMEL luminal domain (Fig. 6c **right panels**). Most of these structures co-localized with LAMP1 in DAPT-treated control cells (and to some extent in DAPT-treated CD63-depleted cells; **Suppl. Fig. S5c**), and IEM analysis of these cells revealed an accumulation of the PMEL cytoplasmic domain in small vesicles, conventional MVEs and lysosomes that were distinct from stage II premelanosomes (labeled for the PMEL luminal domain; Fig. 6d). These observations suggest that if not degraded, the CTF accumulates in lysosomes. Consistent with this conclusion, CTF also accumulated in cells treated with lysosomal protease inhibitors (**Suppl. Fig. S5d**). Targeting to lysosomes required ESCRT-I, because in Tsg101-depleted cells the CTF accumulated in endosomal structures together with the luminal domain (Fig. 6b and. **S5a, b**) and did not localize to LAMP1-positive compartments (**Suppl. Fig. S5c**). These data indicate that the CTF is degraded within the lysosomal pathway and requires ESCRT-I for proper targeting to this pathway.

Endosomal bilayered clathrin- and Hrs-containing coats function in other cell types in ESCRT-dependent sorting of ubiquitinated substrates to ILVs of MVBs for lysosomal degradation (Raiborg et al., 2008; Raiborg et al., 2006; Raposo et al., 2001; Sachse et al., 2002; Theos et al., 2006b). Consistent with such a fate for the CTF, EM of DAPT-treated cells indicates an expansion of bilayered clathrin coats on the cytosolic face of MVEs (Fig. 6e). IEM revealed that the labeling for the CTF was highly enriched in these coated regions (Fig. 6f). Because Hrs binds avidly to ubiquitinated cytosolic domains of transmembrane proteins, we tested whether the CTF was associated with ubiquitylation by immunoprecipitating CTF and other PMEL isoforms from control and DAPT-treated cell lysates and assaying for ubiquitin by immunoblotting. Relative to control cells, in which very little ubiquitin signal was detected in any of the PMEL immunoprecipitates, DAPT treatment resulted in a substantial enrichment of high molecular weight ubiquitin conjugates in immunoprecipitates obtained with αPmel-C but not with antibodies to the PMEL lumenal domain (Fig. 6g). As a control, ubiquitin was associated with MART-1, a known constitutive substrate for ubiquitination (Levy et al., 2005), regardless of DAPT treatment (Fig. 6g). This indicated that either CTF was itself polyubiquitylated or associated with polyubiquitylated proteins. The association of CTF with ubiquitin was only observed in MNT-1 cell lysates prepared with mild detergent (Brij97). When lysates were prepared with Triton X-100, ubiquitylated proteins did not co-precipitate with CTF. This suggest either

that the CTF associates with an ubiquitinated partner in a Triton X-100-sensitive manner or that ubiquinated CTF is only solubilized in mild detergent (not shown).

In the absence of CD63, both PMEL luminal domain and CTF are sorted and degraded in an ESCRT-dependent manner

Because PMEL delivery onto ILVs of coated endosomes is reduced upon CD63 depletion, it was surprising that full-length PMEL did not accumulate either at the limiting membrane of coated endosomes (Fig. 2c) or in cell lysates (Fig. 4b). To determine the fate of PMEL in CD63-depleted MNT-1 cells we first quantified the distribution of its luminal domain by IEM. Relative to control cells, PMEL-luminal domain in CD63-depleted cells was detected in the Golgi apparatus, vesicular profiles, and in electron dense membranous organelles with hallmarks of lysosomes (Fig 7a; illustrated in **Suppl. Fig. S6a**) that accumulate in these cells (see Fig. 3e, f). Interestingly, the PMEL-luminal domain was detected at similar levels on MVEs of control and CD63-depleted cells (Fig. 7a). As compared to conventional EM (Fig. 2d and f) IEM does not always allow to clearly discriminate between coated and non coated MVEs. To define MVEs in which PMEL was sorted in absence of CD63 ultrathin cryosections we double immunogold labeled with HMB50 and an anti-Hrs antibody. In agreement with the conventional EM data showing the presence of ILVs only in non-coated MVEs (Fig 7b left panel), PMEL labeling was observed in MVEs but not in Hrs-positive endosomes, (Fig 7b right panel). In these MVEs, both PMEL-luminal domain and CTF were associated to a large degree with the ILVs that are still generated upon CD63 inactivation **(Suppl. Fig. S6b and c**; see also Fig. 2f). We interpret this observation as evidence that full-length PMEL is delivered to ESCRT-dependent ILVs that continue to form upon CD63 depletion. Consistent with this interpretation, CD63 was not required for ESCRT-dependent ILV sorting and degradation, because steady state levels of the melanocyte transmembrane protein, MART-1 - which is known to be ubiquitinated and sorted to ILVs of MVEs (De Maziere et al., 2002; Levy et al., 2005) - was not altered by CD63 depletion (Fig. 7e). The lack of effect of CD63 depletion on ESCRT-dependent ILV formation was not limited to melanocytic cells, since inactivation of CD63 in HeLa cells did not affect the ESCRT-dependent sorting and degradation of the epidermal growth factor receptor (**Suppl. Fig. S7**).

Our interpretation of these results predicts that CD63 regulates a tight balance between ESCRT-independent and dependent sorting within contiguous membranes of MVEs. Consistent with this prediction, the bilayered coats on the cytosolic face of the MVE limiting membrane were unusually expanded in CD63-depleted cells (Fig. 7c, d), much like our observations in DAPT-treated cells (Fig. 6e). The increase in coated areas correlated with an increased recruitment of Hrs (**Suppl. Fig. S6e, f**) and accumulation of the PMEL luminal domain in coated regions (Fig. 2c). Together, these data suggest that both PMEL luminal domain and CTF are confined within Hrs enriched coats for ESCRT-dependent targeting to the endosomal degradative pathway in the absence of CD63.

To test whether PMEL was degraded in an ESCRT-dependent fashion upon CD63 depletion, we assessed the behavior of PMEL in cells depleted concomitantly for CD63 and the ESCRT-I subunit Tsg101. Whereas levels of detergent-soluble Mα, Mβ and CTF and of total or detergent-insoluble MαC were decreased in lysates of cells treated with CD63 siRNA alone (Fig. 4b, 7e), they were partially or completely restored to control levels upon concomitant treatment with both siRNAs (Fig. 7e). IEM analyses of cells treated with both siRNAs showed that most of the “rescued” PMEL lumenal and CTF domains accumulated at the limiting membrane of enlarged vacuolar compartments (Fig 7f). These data support the interpretation that in the absence of CD63, full-length PMEL becomes a substrate for ESCRT-dependent sorting and ultimate degradation.

Discussion

In this study we show that the TSPAN CD63 is an essential effector of an ESCRT-independent MVE-generating mechanism that is ultimately required to initiate polymerization of PMEL lumenal domains into functional amyloid fibrils. This process reflects a balance between two sorting events operating on contiguous endosomal membranes – ESCRT-independent sorting to ILVs and ESCRT-dependent exclusion from these ILVs (**Suppl. Fig. S8**). Each mechanism differentially sorts distinct functional domains derived from the single cargo protein PMEL. Our data defines CD63 as an important modulator of the balance between these two MVE sorting mechanisms that ultimately destine proteins for LROs or for degradation.

Whereas the involvement of the ESCRT machinery in generating ILVs during MVE biogenesis is well-documented (Hurley, 2008), the only reported “effector” of ESCRT-independent ILV sorting is ceramide in sorting the proteolipid PLP (Trajkovic et al., 2008). We could not obtain evidence for a ceramide requirement in PMEL localization or amyloid formation using sphingomyelinase inhibitors or siRNA-mediated inactivation of acidic type II sphingomyelinase **(Suppl. Fig. S9a, b)**. This suggests that distinct ESCRT-independent mechanisms might operate on MVEs in different cells or for different cargoes, perhaps reflecting multiple MVE subpopulations (Buschow et al., 2009; Simons and Raposo, 2009). Proteins of the TSPAN family were predicted to participate in ESCRT-independent ILV sorting because they are highly enriched in ILVs, even in the absence of functional ESCRT components (Buschow et al., 2009; Simons and Raposo, 2009; Stuffers et al., 2009; Trajkovic et al., 2008; van Niel et al., 2006). Our data now confirm this prediction by showing that (1) the ESCRT-independent cargo PMEL (luminal domain) localizes to CD63-containing ILVs even in ESCRT-I-depleted cells, and (2) ILV formation, PMEL sequestration, and downstream melanosome biogenesis are severely reduced in the absence of CD63 expression. These findings highlight the requirement for the TSPAN CD63 in ESCRT-independent ILV generation of MVEs and for the consequent sorting of a cargo protein.

CD63, unlike other TSPANs such as CD9 or CD81, localizes largely to late endosomes and lysosomes in different cell types (Pols and Klumperman, 2009). Our and other published data (Kallquist et al., 2008; Michaux and Cutler, 2004) show that CD63 in specialized cells is predominantly associated with LROs and their endosomal precursors, suggesting a specific role in LRO formation and/or function as proposed (Pols and Klumperman, 2009). Consistently, whereas lysosomal defects are not detected in CD63 knockout mice (Schroder et al., 2009), these mice do harbor altered LROs, as shown here for melanosomes. Our results show that CD63 localizes not only to endosomes and premelanosomes but also to mature melanosomes. Although our data indicate that CD63 functions in melanosome biogenesis during cargo partitioning in MVEs, we cannot exclude that it may also be involved at later stages of melanogenesis or melanosome transfer through interactions with other cargoes and effectors. Futhermore, CD63 is unique among TSPANs in its ability to specifically interact with LRO cargo partners, such as PMEL (shown here), LMP-1 (Verweij et al., 2011) and the neutrophil elastase in neutrophils (Kallquist et al., 2008). Our data predict that other LRO cargoes will be similarly reliant on CD63 for their partitioning.

While our previous studies showed that effective PMEL sorting to ILVs required the luminal domain (Theos et al., 2006b) and that within MVEs, the luminal domain and CTF were differentially enriched in ILVs and at the limiting membrane, respectively (Raposo et al., 2001), we only detected a physical interaction between CD63 and the PMEL CTF. We speculate that this steady state interaction reflects a transient interaction between CD63 and full-length PMEL, or with Mα-Mβ complexes, on the limiting membrane of vacuolar

endosomes. These data, together with the impact of CD63 depletion on PMEL sorting and downstream amyloidogenic processing, support a model in which the interaction of CD63 with the PMEL CTF stabilizes PMEL within endosomal domains that are rapidly targeted for ESCRT-independent ILV formation. This interaction is likely to be short-lived, with rapid proteolytic release of CTF from Mα and incorporation of Mα onto forming ILVs. This interpretation is consistent with the rapid proteolytic maturation of PMEL in post-Golgi compartments (Berson et al., 2003) and the steady-state enrichment of PMEL lumenal domains within endosomes on ILVs (Berson et al., 2001; Berson et al., 2003; Raposo et al., 2001). Alternatively, the CTF region and luminal domain of PMEL might independently contribute to ESCRT-independent/CD63-dependent ILV sorting. This model would be consistent with the concomitant detection of CD63 and both the lumenal and cytoplasmic domains of PMEL in ILVs in HeLa cells (Berson et al., 2001; Berson et al., 2003), and with the smaller ILV size and incomplete amyloidogenesis associated with a chimeric construct lacking the PMEL cytoplasmic domain (Theos et al., 2006b).

Remarkably, while the CTF appears to facilitate ESCRT-independent sorting by diverting PMEL from the ESCRT machinery, its own fate is to be degraded in an ESCRT-dependent manner. The association of the CTF with ubiquitylated proteins suggests that the CTF might be a passive passenger of the ESCRT pathway. Exactly how the CTF is sorted for degradation is not clear. It is possible that CTF accompanies PMEL luminal domains during invagination onto ILVs, and then becomes reexposed on the endosomal limiting membrane upon back fusion of the ILVs (**Suppl. Fig. S8**); a similar process has been proposed in other cell systems (Falguieres et al., 2008; van Nispen tot Pannerden et al.), and would be consistent with our electron tomography analyses of early melanosomes/MVEs (Hurbain et al., 2008). Alternatively, the CTF could be retained on the MVE membrane after PMEL cleavage and segregation from the luminal domain, which – perhaps by virtue of an affinity for ILV-enriched components – would associate with CD63-dependent ILVs. Either mechanism would expose the isolated CTF, either directly or indirectly in association with an ubiquitylated partner, to ESCRT-containing clathrin coats on the MVE limiting membrane (Raposo et al., 2001; Theos et al., 2006b; Truschel et al., 2009) (**Suppl. Fig. S8**). ESCRT-dependent sorting is likely to be tightly linked to cleavage of the CTF by the gamma secretase, which is required for CTF disposal (this study and (Kummer et al., 2009)). The reported localization and activity of gamma-secretase to the limiting membrane of lysosomes (Pasternak et al., 2003) could reconcile both events. Confirmation of this hypothesis requires further investigations.

Our data have important implications for distinct fates of ILVs that are formed by different mechanisms. We show that whereas the CD63-dependent ILVs bearing PMEL luminal domains are ultimately destined for melanosomes, the CD63-independent, ESCRT-dependent vesicles bearing CTF are destined for degradation (**Suppl. Fig. S8**). The formation of ESCRT-independent ILVs and the sequestration of PMEL CTF in ESCRT-dependent clathrin coats on the cytosolic side of the same endosomal membrane suggests that distinct but concomitant sorting mechanisms are integrated within a single compartment (Buschow et al., 2009; Simons and Raposo, 2009) (**Suppl. Fig. S8**). We propose that a key role for the CD63-dependent pathway is to protect cargoes from ESCRT-dependent degradation. This is supported by the lack of effect of CD63 inactivation on ESCRT-dependent cargoes (EGFR) and by the confinement of ESCRT-independent cargoes (PMEL luminal domain) to clathrin and Hrs-positive coats for subsequent ESCRT-dependent degradation in absence of CD63. (Fig. 2C and **Fig. S6**). Whether degradative MVEs mature from clathrin-coated subdomains or are distinct compartments will require further study. The data further support a function for CD63 in maintaining a tight balance that controls the exclusive fate and sorting of a single cargo by an ESCRT-dependent or -independent pathway. This CD63-dependent segregation of LRO cargoes from cargoes destined for

degradation might then explain the association of CD63 with multiple LROs (Raposo et al., 2007).

Finally, we show that the loss of ESCRT-independent PMEL sorting in CD63-depleted cells is accompanied by a diminution of PMEL amyloid formation. This is consistent with a model in which MVEs provide an environment conducive for the proteolytic processing and unfolding of amyloidogenic precursors, supported by our previous observations by high resolution by electron tomography (Hurbain et al., 2008) and studies by others (Kovacs et al., 2007). The link between ILV formation, the TSPAN CD63 and the generation of physiological PMEL amyloid opens a new avenue for further understanding the mechanisms underlying the formation of amyloid in pathological models.

Experimental Procedures

Antibodies

Monoclonal antibodies and their sources were as follows. Mouse monoclonal antibodies TA99 to Tyrp1 (ab3312; used for IFM), HMB45 to PMEL (ab787), M2-7C10 to MART-1 (ab3168), and anti-neutral sphingomyelinase (ab55711), rabbit polyclonal anti-β-tubulin (ab6046), and horseradish peroxidase (HRP)-conjugated goat polyclonal antibodies to rabbit IgG (ab6721) and to mouse IgG (ab6789) were from Abcam. Mouse anti-CD63 used for IEM was from Zymed/Invitrogen. Mouse monoclonal antibody P4D1 to ubiquitin (sc-8017) and rabbit polyclonal anti-Tyrp1 (sc-25543; used for western blotting) were from Santa Cruz Biotechnology, Inc. Mouse monoclonal antibodies H4A3 to human LAMP-1 from BD Biosciences, HMB50 to PMEL from Neomarkers (Fremont, Ca), and 4A10 to Tsg101 from GeneTex were used as described. Polyclonal sheep anti-EGF receptor was from Interchim. Affinity-purified anti-peptide antibodies recognizing the PMEL N-terminus (αPmel-N) (Berson et al 2003), C-terminus (aPmel-C) (Raposo et al., 2001) and PKD domain (I51 - a kind gift of P. Cresswell, N. Vigneron, and R. M. Leonhardt, Yale Univ., New Haven, CT) (Watt et al., 2009) were described previously. Mouse monoclonal antibodies to CD81, CD55, CD9 and CD63 used for immunoblotting, immunoprecipitation and IFM were described previously (Abache et al., 2007). Antibody to Hrs was a kind gift S. Urbe. Secondary goat anti-rabbit or anti-mouse antibodies conjugated to Alexa Fluor-488- or 555- or 647 were from Invitrogen. Protein A conjugated to 10 or 15 nm gold particles (PAG10, PAG15) were from Cell Microscopy Center (AZU, Utrecht University, Utrecht, The Netherlands).

Cell culture, drug and EGF treatment, transfection and siRNA depletion

Human melanocytic MNT-1 cells and HeLa cells were maintained as previously described (Berson et al., 2001; Raposo et al., 2001). Cells were treated for 24hrs with 1μM DAPT (Sigma) or with 2,5μM GW4869 (Sigma) or with a cocktail of lysosomal proteases inhibitors Leupeptin, Ca-074Me and pepstatin A (10 μg/ml) (Sigma). For EGF pulse chase, cells were starved for 4hrs in serum free cell culture medium and pulsed with EGF-biotin at 50 ng/ml (Invitrogen) for 30min at 37 °C. Cells were then washed and chased at 37 °C with serum free cell culture medium. HeLa cells were transfected with plasmid constructs using Lipofectamine 2000 (Invitrogen) following the manufacturer's recommendations and cells were collected and analyzed 48 h after transfection. MNT-1 cells were transduced with siRNA duplex oligonucleotides as reported (Theos et al., 2006b). Cells were subjected to one round of siRNA transduction and processed at day 3.

The sense strands for the indicated double stranded siRNAs (21-mers) were synthesized with the following sequences or derived from the following references. siRNA CD63 #1: 5′-GTT CTT GCT CTA CGT CCT C -3′; siRNA CD63 #2: 5′-CAG ATG GAG AAT TAC

CCG AAA -3′ (Hs_CD63_6_HP siRNA from QIAGEN); siRNA CD81: 5′-GCA CCA AGT GCA TCA AGT A -3′; siRNA neutral sphingomyelinase: 5′-CCG CAT TGA CTA CGT GCT TTA -3′ (Hs_SMPD2_5_HP from QIAGEN); siRNA presenilin-1: 5′-CAG GCA TAT CTC ATT ATG ATT -3′ (Hs_PSEN1_11_HP Validated from QIAGEN); siRNA presenilin-2: 5′-CAG GAG AGA AAT GAG CCC ATA -3′ (Hs_PSEN2_5_HP Validated from QIAGEN); siRNA non-targeting control: 5′-AAT TCT CCG AAC GTG TCA CGT -3′. (from QIAGEN) siRNA Tsg101: 5′-GGA GGU CAG AAG AGA GCA G -3′ (from Garrus et al Cell 2001). Full length PMEL WT cDNA has been described in (Theos et al., 2006b).

Western blot

MNT-1 cells at 80% confluency were washed in cold PBS and lysed on ice in lysis buffer (50 mM Tris, 150 mM NaCl, 0.1% (v/v) Triton X-100, 10 mM EDTA, pH 7.2, 10 mM N-ethylmaleimide (Sigma), 5 mM oxidized gluthatione (Calbiochem) and protease inhibitor cocktail (Roche). Triton X-100 insoluble material was obtained as previously described (Berson et al., 2001). Lysates were incubated in sample buffer with or without 350 mM 2-mercapthethanol (Sigma), boiled for 5 min, and fractionated by SDS-PAGE using Nupage (3–8%) Tris-Acetate gels (Invitrogen) or Nupage (4–12%) Bis-Tris gels (Invitrogen) and transferred onto nitrocellulose membranes (Millipore). The membranes were blocked in PBS/0.1%Tween-20 (PBS/T) with 5% non-fat dried milk, incubated with indicated primary antibody diluted in PBS/T, washed four times in blocking solution, and finally incubated with HRP-conjugated secondary antibody followed by washing in PBS/T. Blots were developed using the ECL Plus Western blotting detection system (GE Healthcare) according to the manufacturer's instruction. Signal intensities were quantified with Image J software.

For immunoprecipitation and corresponding Western blot, cells were lysed directly in lysis buffer (30 mM Tris pH 7.4, 150 mM NaCl, 1 mM $CaCl_2$, 1 mM $MgCl_2$ and 0.02% NaN_3) containing 1% (w/v) Brij97 (Sigma, St Louis, MO) and proteases inhibitors. After 30 min at 4°C, insoluble material was removed by centrifugation at 12,000g and cell lysate was precleared for 2 h by addition of 1/1000 volume heat inactivated goat serum and 20 μl protein G-sepharose beads (Amersham Bioscience). Proteins were then immunoprecipitated by adding 2 μg specific antibody and 10 μl protein G sepharose beads to 200–400 μl lysate. After 2 h incubation at 4°C under constant agitation, beads were washed five times in lysis buffer containing 1% Brij97. The immunoprecipitates were fractionated by 5–15% SDS-PAGE under non-reducing or reducing conditions and transferred to a nitrocellulose membrane (Amersham Bioscience). Membranes were probed as described above, except for Biotin-labelled primary antibodies (anti-CD63; anti-CD81) where AlexaFluor 680-streptavidin conjugates or AlexaFlour 800- streptavidin conjugates (Invitrogen) were used for detection and blots were developed using the Odyssey Infrared Imaging System (LI-COR Biosciences).

Immunofluorescence microscopy (IFM)

Untreated, drug-treated, or transfected MNT-1 cells on coverslips were rinsed in PBS and fixed for 15 min in 4% paraformaldehyde/PBS at room temperature (RT). Fixed cells were washed in PBS and quenched 10 min in PBS/50 mM glycine, saturated in PBS containing 1 mg/ml BSA (blocking buffer), and permeabilized in PBS/0.05% saponin/1 mg/ml BSA (incubation buffer, IB). Cells were incubated 1 h with the primary antibody diluted in IB, washed three times in IB and incubated with the corresponding secondary anti-rabbit and anti-mouse antibodies conjugated to Alexa 488 or Alexa 568 (Molecular Probes/Invitrogen) diluted in IB for 45 min. Coverslips were washed three times with IB and then mounted in DABCO medium and examined on a Leica Microsystem (Nanterre, France) DM-RXA2 3D deconvolution microscope equipped with a piezo z-drive (Physik Instrument, Pantin, France) and a 100x 1.4NA PL-APO objective lens. Images are maximum-intensity z

projections of 3D image stacks (except FIgure 5D, which shows a single deconvolved layer) acquired every 0,2μm using Metamorph software (MDS Analytical Technologies, Sunnyvale, CA) and a Coolsnap HQ (Photometrics Coolsnap HQ) cooled CCD-camera.

Electron Microscopy

For conventional EM of MNT-1 cells, cells grown on coverslips were fixed with 2.5% glutaraldehyde in 0.1 M cacodylate buffer for 24 h and processed for epon embedding as described (Raposo et al., 2001). For EM analysis of RPE sections, tissues from two CD63−/− mice (aged 2 months) and two age-matched wild-type mice were fixed by perfusion of the mice with glutaraldehyde (6% in PBS). Tissue blocks from the eyes were processed for epon embedding and ultrathin sections were contrasted with uranyl acetate and lead citrate as described (Lopes et al., 2007). For ultrathin cryosectioning and immunogold labeling, cells were fixed with 2% PFA or with a mixture of 2% PFA and 0.2% glutaraldehyde in 0.1 M phosphate buffer, pH 7.4. Cells were processed for ultracryomicrotomy and single or double immunogold labeled using PAG10 or PAG15 as reported (Raposo et al., 2001). All samples were analyzed using a FEI CM120 electron microscope (FEI Company), and digital acquisitions were made with a numeric camera (Keen View; Soft Imaging System, SIS, Germany).

Image Analysis and quantification

Quantification of immunogold labeling on ultrathin cryosections was performed as described previously (Delevoye et al., 2009). Melanin content was performed as described (Wasmeier et al., 2006). The relative distribution of PMEL luminal and CD63 in MNT-1 cells was evaluated by direct EM analysis of randomly selected cell profiles from two distinct grids. More than 1500 gold particles for each condition were counted and assigned to the compartment over which they were located. For quantification of distinct compartments in siRNA-treated cells and controls, each of the compartments was defined by its morphology and by correlation with immunogold labeling for different organelle-markers (EEA1 and Hrs for early endosomes, TGN46 for the TGN, LAMP-1 for late endosomes/lysosomes) and internalized endocytic tracers (BSA-gold and Tf-FITC for endosomes of different maturation stage) as previously described (Raposo et al., 2001). MVBs or MVEs were defined as compartments delimited by a membrane with numerous internal vesicles; coated MVEs have few internal vesicles and an electron dense coat on at least one face of the limiting membrane. Electron-dense compartments with no or few internal membranes were classified as lysosomes. Melanosome stages were defined by morphology (Raposo et al., 2001) (Seiji et al., 1963). Quantification of PMEL luminal domain distribution in MVEs of MNT-1 cells was performed on single immunogold labeled cryosections by counting the number of gold particles on the limiting membrane and on ILVs. Labeling was considered to be associated with the limiting membrane when the gold particle was within 20 nm of the limiting membrane and with no cross-sectioned ILVs in the direct vicinity. Results are presented as a percentage of the total number of gold particles on ILVs in each compartment and represent a mean and standard deviation of three independent experiments. Quantification of average diameter of MVEs and the length of clathrin coat was determined using the iTEM software (Soft Imaging System, SIS, Germany).

Acknowledgments

We are grateful to D. Tenza, I. Hurbain, C. Delevoye, S Held, B Watt and Renate Lüllmann-Rauch for technical help, insightful discussions during the course of this work and critical reading of the manuscript. We are grateful to V. Fraisier and L. Sengmanivong (PITC-IBiSA Imaging Facility, Institut Curie) for assistance with deconvolution microscopy. This work was supported by Institut Curie, CNRS, Fondation pour la Recherche Medicale Association pour la Recherche sur le Cancer (to GR), the Deutsche Forschungsgemeinschaft (to P.S.) and NIH grant R01 AR048155 (to MSM).

References

Abache T, Le Naour F, Planchon S, Harper F, Boucheix C, Rubinstein E. The transferrin receptor and the tetraspanin web molecules CD9, CD81, and CD9P-1 are differentially sorted into exosomes after TPA treatment of K562 cells. J Cell Biochem. 2007; 102:650–664. [PubMed: 17407154]

Berson JF, Harper DC, Tenza D, Raposo G, Marks MS. Pmel17 initiates premelanosome morphogenesis within multivesicular bodies. Mol Biol Cell. 2001; 12:3451–3464. [PubMed: 11694580]

Berson JF, Theos AC, Harper DC, Tenza D, Raposo G, Marks MS. Proprotein convertase cleavage liberates a fibrillogenic fragment of a resident glycoprotein to initiate melanosome biogenesis. J Cell Biol. 2003; 161:521–533. [PubMed: 12732614]

Buschow SI, Nolte-'t Hoen EN, van Niel G, Pols MS, ten Broeke T, Lauwen M, Ossendorp F, Melief CJ, Raposo G, Wubbolts R, et al. MHC II in dendritic cells is targeted to lysosomes or T cell-induced exosomes via distinct multivesicular body pathways. Traffic. 2009; 10:1528–1542. [PubMed: 19682328]

Charrin S, le Naour F, Silvie O, Milhiet PE, Boucheix C, Rubinstein E. Lateral organization of membrane proteins: tetraspanins spin their web. Biochem J. 2009; 420:133–154. [PubMed: 19426143]

de Gassart A, Geminard C, Fevrier B, Raposo G, Vidal M. Lipid raft-associated protein sorting in exosomes. Blood. 2003; 102:4336–4344. [PubMed: 12881314]

De Maziere AM, Muehlethaler K, van Donselaar E, Salvi S, Davoust J, Cerottini JC, Levy F, Slot JW, Rimoldi D. The melanocytic protein Melan-A/MART-1 has a subcellular localization distinct from typical melanosomal proteins. Traffic. 2002; 3:678–693. [PubMed: 12191019]

Delevoye C, Hurbain I, Tenza D, Sibarita JB, Uzan-Gafsou S, Ohno H, Geerts WJ, Verkleij AJ, Salamero J, Marks MS, et al. AP-1 and KIF13A coordinate endosomal sorting and positioning during melanosome biogenesis. J Cell Biol. 2009; 187:247–264. [PubMed: 19841138]

Falguieres T, Luyet PP, Bissig C, Scott CC, Velluz MC, Gruenberg J. In vitro budding of intralumenal vesicles into late endosomes is regulated by Alix and Tsg101. Mol Biol Cell. 2008; 19:4942–4955. [PubMed: 18768755]

Fang Y, Wu N, Gan X, Yan W, Morrell JC, Gould SJ. Higher-order oligomerization targets plasma membrane proteins and HIV gag to exosomes. PLoS Biol. 2007; 5:e158. [PubMed: 17550307]

Fowler DM, Koulov AV, Alory-Jost C, Marks MS, Balch WE, Kelly JW. Functional amyloid formation within mammalian tissue. PLoS Biol. 2006; 4:e6. [PubMed: 16300414]

Gruenberg J, Stenmark H. The biogenesis of multivesicular endosomes. Nat Rev Mol Cell Biol. 2004; 5:317–323. [PubMed: 15071556]

Harper DC, Theos AC, Herman KE, Tenza D, Raposo G, Marks MS. Premelanosome amyloid-like fibrils are composed of only golgi-processed forms of Pmel17 that have been proteolytically processed in endosomes. J Biol Chem. 2008; 283:2307–2322. [PubMed: 17991747]

Hoashi T, Muller J, Vieira WD, Rouzaud F, Kikuchi K, Tamaki K, Hearing VJ. The repeat domain of the melanosomal matrix protein PMEL17/GP100 is required for the formation of organellar fibers. J Biol Chem. 2006; 281:21198–21208. [PubMed: 16682408]

Hoashi T, Watabe H, Muller J, Yamaguchi Y, Vieira WD, Hearing VJ. MART-1 is required for the function of the melanosomal matrix protein PMEL17/GP100 and the maturation of melanosomes. J Biol Chem. 2005; 280:14006–14016. [PubMed: 15695812]

Hurbain I, Geerts WJ, Boudier T, Marco S, Verkleij AJ, Marks MS, Raposo G. Electron tomography of early melanosomes: implications for melanogenesis and the generation of fibrillar amyloid sheets. Proc Natl Acad Sci U S A. 2008; 105:19726–19731. [PubMed: 19033461]

Hurley JH. ESCRT complexes and the biogenesis of multivesicular bodies. Curr Opin Cell Biol. 2008; 20:4–11. [PubMed: 18222686]

Kallquist L, Hansson M, Persson AM, Janssen H, Calafat J, Tapper H, Olsson I. The tetraspanin CD63 is involved in granule targeting of neutrophil elastase. Blood. 2008; 112:3444–3454. [PubMed: 18669870]

Katzmann DJ. No ESCRT to the Melanosome: MVB Sorting without Ubiquitin. Dev Cell. 2006; 10:278–280. [PubMed: 16516831]

Kovacs GG, Gelpi E, Strobel T, Ricken G, Nyengaard JR, Bernheimer H, Budka H. Involvement of the endosomal-lysosomal system correlates with regional pathology in Creutzfeldt-Jakob disease. J Neuropathol Exp Neurol. 2007; 66:628–636. [PubMed: 17620988]

Kummer MP, Maruyama H, Huelsmann C, Baches S, Weggen S, Koo EH. Formation of Pmel17 amyloid is regulated by juxtamembrane metalloproteinase cleavage, and the resulting C-terminal fragment is a substrate for gamma-secretase. J Biol Chem. 2009; 284:2296–2306. [PubMed: 19047044]

Kushimoto T, Basrur V, Valencia J, Matsunaga J, Vieira WD, Ferrans VJ, Muller J, Appella E, Hearing VJ. A model for melanosome biogenesis based on the purification and analysis of early melanosomes. Proc Natl Acad Sci U S A. 2001; 98:10698–10703. [PubMed: 11526213]

Levy F, Muehlethaler K, Salvi S, Peitrequin AL, Lindholm CK, Cerottini JC, Rimoldi D. Ubiquitylation of a melanosomal protein by HECT-E3 ligases serves as sorting signal for lysosomal degradation. Mol Biol Cell. 2005; 16:1777–1787. [PubMed: 15703212]

Lopes VS, Wasmeier C, Seabra MC, Futter CE. Melanosome maturation defect in Rab38-deficient retinal pigment epithelium results in instability of immature melanosomes during transient melanogenesis. Mol Biol Cell. 2007; 18:3914–3927. [PubMed: 17671165]

Michaux G, Cutler DF. How to roll an endothelial cigar: the biogenesis of Weibel-Palade bodies. Traffic. 2004; 5:69–78. [PubMed: 14690496]

Pasternak SH, Bagshaw RD, Guiral M, Zhang S, Ackerley CA, Pak BJ, Callahan JW, Mahuran DJ. Presenilin-1, nicastrin, amyloid precursor protein, and gamma-secretase activity are co-localized in the lysosomal membrane. The Journal of biological chemistry. 2003; 278:26687–26694. [PubMed: 12736250]

Pols MS, Klumperman J. Trafficking and function of the tetraspanin CD63. Exp Cell Res. 2009; 315:1584–1592. [PubMed: 18930046]

Raiborg C, Malerod L, Pedersen NM, Stenmark H. Differential functions of Hrs and ESCRT proteins in endocytic membrane trafficking. Exp Cell Res. 2008; 314:801–813. [PubMed: 18031739]

Raiborg C, Stenmark H. The ESCRT machinery in endosomal sorting of ubiquitylated membrane proteins. Nature. 2009; 458:445–452. [PubMed: 19325624]

Raiborg C, Wesche J, Malerod L, Stenmark H. Flat clathrin coats on endosomes mediate degradative protein sorting by scaffolding Hrs in dynamic microdomains. J Cell Sci. 2006; 119:2414–2424. [PubMed: 16720641]

Raposo G, Marks MS. Melanosomes--dark organelles enlighten endosomal membrane transport. Nat Rev Mol Cell Biol. 2007; 8:786–797. [PubMed: 17878918]

Raposo G, Marks MS, Cutler DF. Lysosome-related organelles: driving post-Golgi compartments into specialisation. Curr Opin Cell Biol. 2007; 19:394–401. [PubMed: 17628466]

Raposo G, Tenza D, Murphy DM, Berson JF, Marks MS. Distinct protein sorting and localization to premelanosomes, melanosomes, and lysosomes in pigmented melanocytic cells. J Cell Biol. 2001; 152:809–824. [PubMed: 11266471]

Sachse M, Urbe S, Oorschot V, Strous GJ, Klumperman J. Bilayered clathrin coats on endosomal vacuoles are involved in protein sorting toward lysosomes. Mol Biol Cell. 2002; 13:1313–1328. [PubMed: 11950941]

Schroder J, Lullmann-Rauch R, Himmerkus N, Pleines I, Nieswandt B, Orinska Z, Koch-Nolte F, Schroder B, Bleich M, Saftig P. Deficiency of the tetraspanin CD63 associated with kidney pathology but normal lysosomal function. Mol Cell Biol. 2009; 29:1083–1094. [PubMed: 19075008]

Seiji M, Shimao K, Birbeck MS, Fitzpatrick TB. Subcellular localization of melanin biosynthesis. Ann N Y Acad Sci. 1963; 100:497–533. [PubMed: 13992624]

Simons M, Raposo G. Exosomes--vesicular carriers for intercellular communication. Curr Opin Cell Biol. 2009; 21:575–581. [PubMed: 19442504]

Stuffers S, Sem Wegner C, Stenmark H, Brech A. Multivesicular endosome biogenesis in the absence of ESCRTs. Traffic. 2009; 10:925–937. [PubMed: 19490536]

Theos AC, Berson JF, Theos SC, Herman KE, Harper DC, Tenza D, Sviderskaya EV, Lamoreux ML, Bennett DC, Raposo G, et al. Dual loss of ER export and endocytic signals with altered

melanosome morphology in the silver mutation of Pmel17. Mol Biol Cell. 2006a; 17:3598–3612. [PubMed: 16760433]

Theos AC, Truschel ST, Raposo G, Marks MS. The Silver locus product Pmel17/gp100/Silv/ME20: controversial in name and in function. Pigment Cell Res. 2005; 18:322–336. [PubMed: 16162173]

Theos AC, Truschel ST, Tenza D, Hurbain I, Harper DC, Berson JF, Thomas PC, Raposo G, Marks MS. A lumenal domain-dependent pathway for sorting to intralumenal vesicles of multivesicular endosomes involved in organelle morphogenesis. Dev Cell. 2006b; 10:343–354. [PubMed: 16516837]

Trajkovic K, Hsu C, Chiantia S, Rajendran L, Wenzel D, Wieland F, Schwille P, Brugger B, Simons M. Ceramide triggers budding of exosome vesicles into multivesicular endosomes. Science. 2008; 319:1244–1247. [PubMed: 18309083]

Truschel ST, Simoes S, Setty SR, Harper DC, Tenza D, Thomas PC, Herman KE, Sackett SD, Cowan DC, Theos AC, et al. ESCRT-I function is required for Tyrp1 transport from early endosomes to the melanosome limiting membrane. Traffic. 2009; 10:1318–1336. [PubMed: 19624486]

van Niel G, Porto-Carreiro I, Simoes S, Raposo G. Exosomes: a common pathway for a specialized function. J Biochem (Tokyo). 2006; 140:13–21. [PubMed: 16877764]

van Nispen tot Pannerden HE, Geerts WJ, Kleijmeer MJ, Heijnen HF. Spatial organization of the transforming MHC class II compartment. Biol Cell. 102:581–591. [PubMed: 20712599]

Verweij FJ, van Eijndhoven MA, Hopmans ES, Vendrig T, Wurdinger T, Cahir-McFarland E, Kieff E, Geerts D, van der Kant R, Neefjes J, et al. LMP1 association with CD63 in endosomes and secretion via exosomes limits constitutive NF-kappaB activation. The EMBO journal. 2011

Vidal M, Mangeat P, Hoekstra D. Aggregation reroutes molecules from a recycling to a vesicle-mediated secretion pathway during reticulocyte maturation. J Cell Sci. 1997; 110(Pt 16):1867–1877. [PubMed: 9296387]

Wakabayashi T, Craessaerts K, Bammens L, Bentahir M, Borgions F, Herdewijn P, Staes A, Timmerman E, Vandekerckhove J, Rubinstein E, et al. Analysis of the gamma-secretase interactome and validation of its association with tetraspanin-enriched microdomains. Nature cell biology. 2009; 11:1340–1346.

Wasmeier C, Romao M, Plowright L, Bennett DC, Raposo G, Seabra MC. Rab38 and Rab32 control post-Golgi trafficking of melanogenic enzymes. J Cell Biol. 2006; 175:271–281. [PubMed: 17043139]

Watt B, van Niel G, Fowler DM, Hurbain I, Luk KC, Stayrook SE, Lemmon MA, Raposo G, Shorter J, Kelly JW, et al. N-terminal domains elicit formation of functional Pmel17 amyloid fibrils. J Biol Chem. 2009; 284:35543–35555. [PubMed: 19840945]

Highlights

- Depletion of CD63 inhibits ESCRT independent sorting of the PMEL luminal domain to ILVs.
- CD63 depletion inhibits the formation of PMEL derived amyloid fibers *in vitro* and *in vivo.*
- PMEL C-terminal fragment is degraded in an ESCRT-dependent manner.
- The PMEL luminal domain becomes sensitive to ESCRT-dependent degradation in CD63-depleted cells.

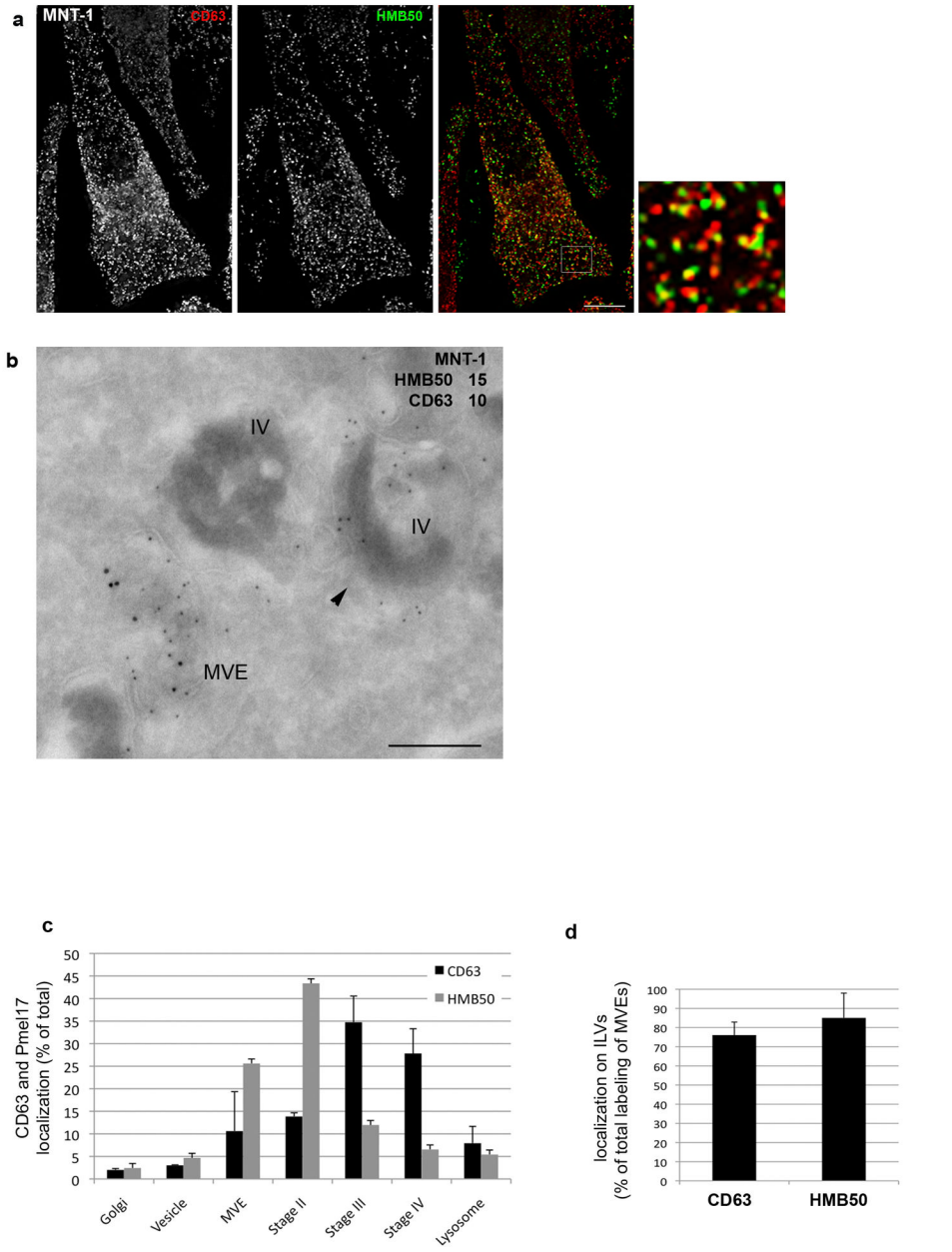

Figure 1. CD63 co-localizes with PMEL on ILVs of MVEs from human melanocytic cells

a. MNT-1 cells were analyzed by IFM after labeling for CD63 and for PMEL using antibody HMB50 (detects the luminal domain). Individual labels, a merged image, and a 3-fold magnification of the merged image are shown. Note that labeling for CD63 and PMEL luminal domain partially overlap. Scale bar, 10 μm. **b-d.** MNT-1 cells were processed for ultrathin cryosectioning and double immunogold labeled for PMEL luminal domain (HMB50; PAG 15) and CD63 (PAG 10). **b.** PMEL and CD63 are both present in MVEs (annoted MVE on the micrograph) whereas only CD63 is observed on maturing melanosomes (annoted IV on the micrograph). Scale bar, 200 nm. **c.** Quantification of immunogold labeling for PMEL (using HMB50 antibody) and CD63. An equivalent number of gold particles representing labeling for PMEL and for CD63 in the EM analysis was counted and assigned to the indicated compartments, which were identified by morphology.

Data are presented as the mean percentage of total gold particles in each compartment +/− SD. **d.** Quantification of immunogold labeling on ILVs vs. the limiting membrane on coated MVEs. Results are expressed as the mean percentage of gold particles (+/− SD) on ILVs (see *b* left panel for an example) relative to total gold particles counted in MVEs.

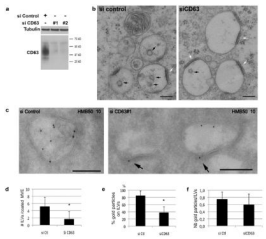

Figure 2. Depletion of CD63 inhibits sorting of PMEL onto ILVs

a. Western blot analysis of lysates of MNT-1 cells treated with control or 2 different CD63 siRNA using anti-CD63 antibody and anti-β-tubulin antibody as a loading control. **b**. MNT-1 cells treated with control or CD63 siRNA #1 were analyzed by conventional EM. Black arrows indicate the ILVs; white arrows indicate the cytosolic bilayered coats. Scale bar, 200 nm. **c.** Ultrathin cryosections of MNT-1 cells treated with control (left panel) or CD63#1 siRNA (right panel) were immunogold labeled for PMEL luminal domain with HMB50 and PAG10. Examples of MVEs from each sample are shown. Whereas in control cells labeling for PMEL luminal domain is associated with the ILVs, in CD63 depleted cells the labeling is observed at the limiting membrane of the endosome close or within the clathrin coat (arrows). Scale bar, 200 nm. **d.** The average number of ILVs (+/− SD) per coated MVE in 50 conventional EM profiles of each sample was quantified. *, $p<0.05$. **e.** Quantification of immunogold labeling for PMEL on ILVs of 100 MVEs is expressed as the mean percentage of gold particles (+/− SD) on ILVs relative to total gold particles in MVEs. *, $p<0.05$. **f.** Same as **e**., but results are expressed as the mean number of gold particles (+/− SD) per ILV within MVEs.

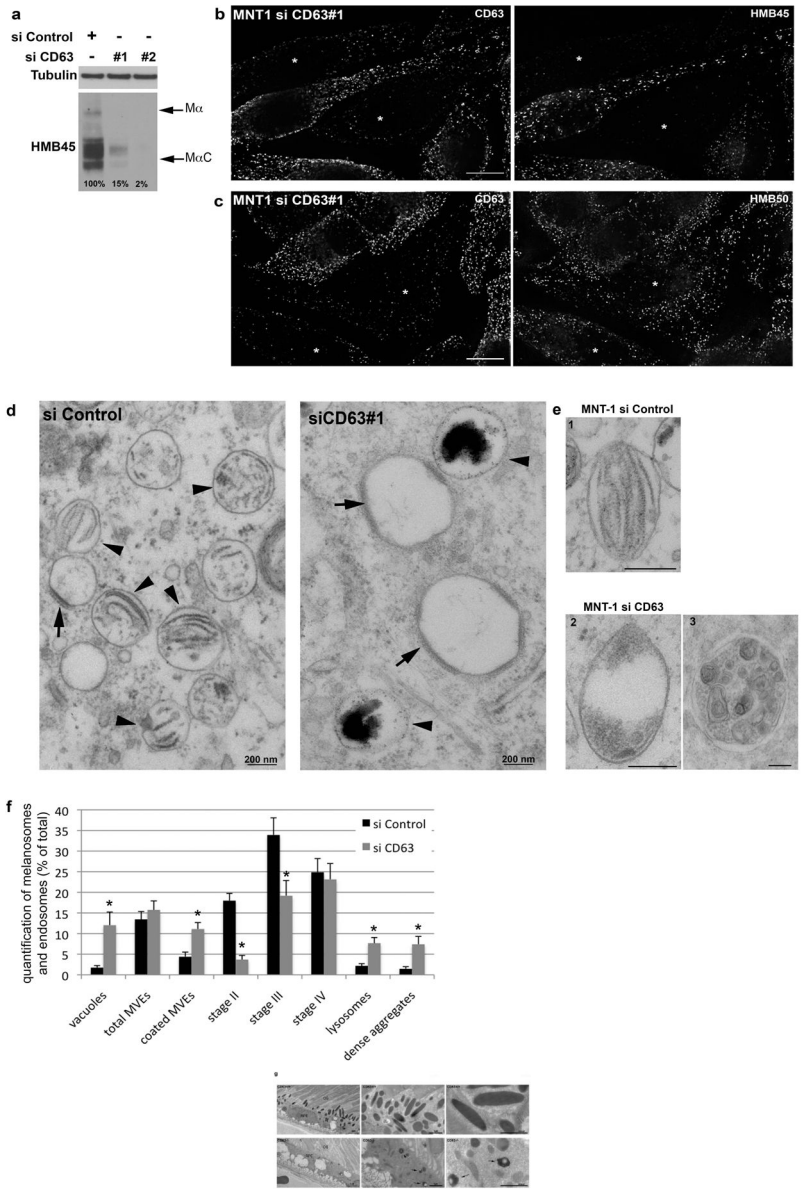

Figure 3. Depletion of CD63 inhibits formation of PMEL fibrils *in vitro* and *in vivo*

a. Triton X-100-insoluble fraction from MNT-1 cells treated with control or 2 different CD63 siRNA (CD63#1 and CD63#2) were analyed by western blot using HMB45 or β-tubulin antibody as a loading control. The percentage of signal intensity relative to the control is noted below each band. **b**, **c.** MNT-1 cells treated with the CD63#1 siRNA were analyzed by IFM after labeling for CD63 and HMB45 (**b**) or HMB50 (**c**). CD63-inactivated cells are indicated by white stars; the micrographs were choosen to better emphasize the differences between CD63-inactivated cells and CD63-expressing cells. Scale bar, 10 μm **d.** MNT-1 cells treated with control or CD63#1 siRNA were analyzed by conventional EM. Arrows, bilayered coats on MVEs; arrowheads, maturing melanosomes (stage II and III). Scale bar, 200 nm. **e.** Representative images of (1) stage II pre-melanosomes in control cells, and (2) dense unstructured aggregates or (3) lysosomes in CD63-depleted cells. Scale bar, 200 nm. **f.** Quantification of the number of different endosomal/melanosomal compartments, as indicated on the X axis and defined by morphology, observed by conventional EM in

MNT-1 cells treated with control and CD63 siRNA. Values represent the percentage of each compartment relative to all of the endosomal/melanosomal compartments identified in 50 cell profiles per condition. Note that “total MVEs” refers to all compartments with internal vesicles within their lumen, whereas “coated MVEs” refers only to early endosomes/stage I melanosomes with a coat on the cytosolic side whatever the number of internal vesicles within their lumen. **g.** Eyes sections from CD63+/+ (top panel) and CD63−/− mice (bottom panel) were analyzed by conventional EM. Shown are regions of the RPE and photoreceptor outer segments (OS). Note the ellipsoidal melanosomes in RPE of CD63+/+ mice, and the electron dense rounder structures (arrows) in the RPE of CD63−/− mice. Scale bars are indicated on each micrograph.

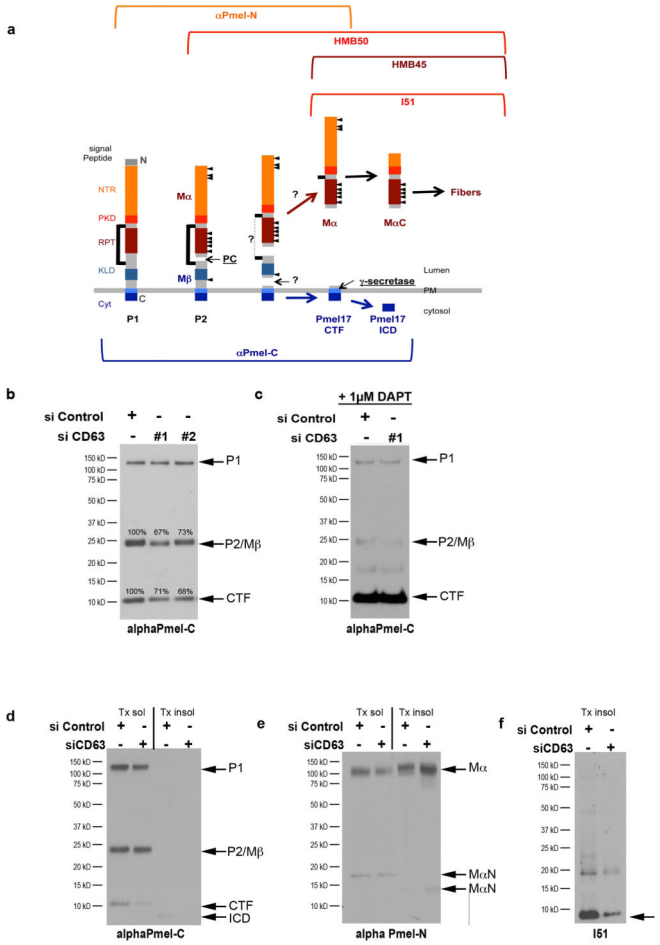

Figure 4. Depletion of CD63 affects the processing of PMEL

a. Schematic representation of PMEL maturation and the epitopes recognized by the antibodies used in this study. The maturation process is described in the text. Black triangles, mature N- and O-linked glycosylation; black bar, a disulfide bond that links Ma and Mb; PC, proprotein convertase; **?**, unknown proteases that cleave Mα to MαC; ICD, intracellular domain of CTF. The names of the anti-PMEL antibodies used in this study and the isoforms they recognize are indicated. **b.** Whole cell lysates of MNT-1 cells treated with control or CD63 siRNA #1 or #2 were analyzed by western blot using αPmel-C antibody. The percentage of signal intensity relative to the control is noted above each band. **c.** Whole cell lysates of MNT-1 cells treated with control or CD63 siRNA#1 and with 1μM DAPT for 4hrs were analyzed by western blot using αPmel-C antibody. **d, e, f.** Triton X-100- soluble (Tx sol) and -insoluble (Tx insol) lysates of MNT-1 cells treated with control or CD63 siRNA#1 were analyzed by western blot using αPmel-C (**d**), αPmel-N (**e**) or I51 antibody (**f**).

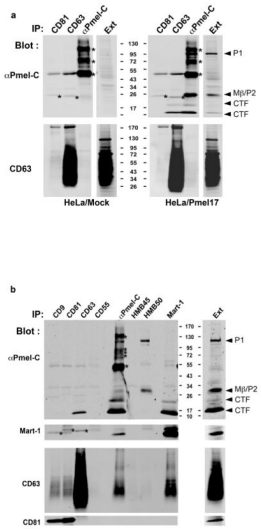

Figure 5. CD63 interacts with PMEL CTF

a. HeLa cells that were mock transfected (left panel) or transfected with PMEL expression vector (right) were lysed in buffer containing 1% Brij97, and lysates were immunoprecipitated with antibodies to CD63, CD81, or PMEL (with αPmel-C) as indicated. Immunoprecipitates or untreated lysate (Ext) were analyzed by western blot with αPmel-C (top panels) or anti-CD63 antibody (bottom panels). **b**. Lysates of MNT-1 cells that were treated for 24 hrs with 1 μM DAPT and lysed with 1% Brij97 were immunoprecipitated with antibodies to TSPANs CD9, CD81, CD63 or CD55, to MART-1, or to PMEL using αPmel-C, HMB45 or HMB50. Immunoprecipitates or untreated lysate (Ext) were fractionated by reducing (top 2 panels) or non-reducing (bottom 2 panels) SDS-PAGE and analyzed by immunoblot with αPmel-C, anti-MART-1, anti-CD63 or anti-CD81.

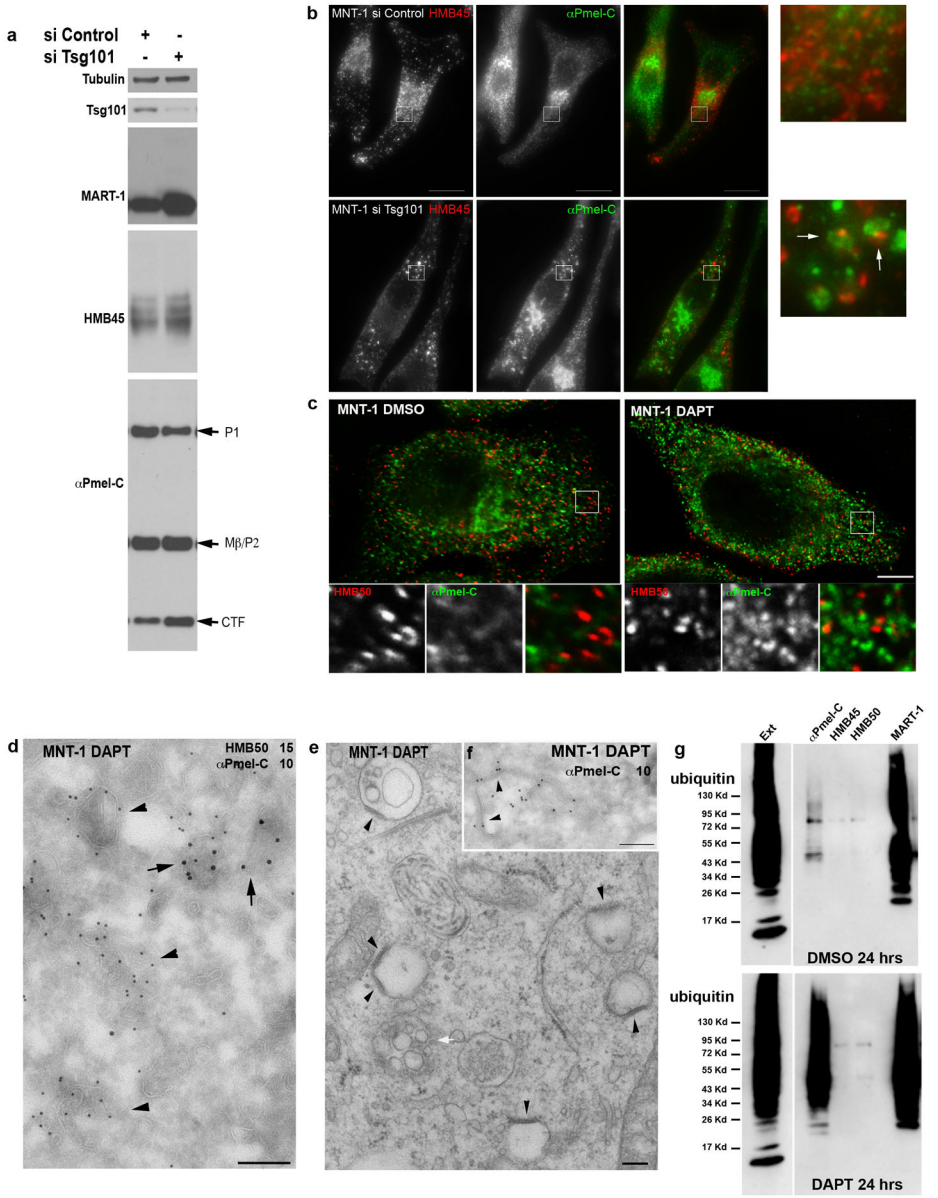

Figure 6. The PMEL CTF is excluded from melanosomes and degraded in an ESCRT-I dependent manner

a. MNT-1 cells treated with control or Tsg101 siRNA were analyzed by western blot using antibodies to β-tubulin, Tsg101, MART-1, or the anti-PMEL antibodies HMB45 and αPmel-C. Only relevant bands are shown. **b.** MNT-1 cells treated with control or Tsg101 siRNA were analyzed by IFM after labeling for HMB45 (red) and αPmel-C (green). White arrows indicate accumulation of αPmel-C labeling around HMB45 positive spots. Individual labels, a merged image, and a 3X magnification of the merged images are shown. Scale bar, 10 μm **c–f.** MNT-1 cells were treated with DMSO or 1 μM DAPT for 4hrs. **c.** Cells were analyzed by IFM after labeling with HMB50 (red) and αPmel-C (green). Scale bar, 10 μm **d.** Ultrathin cryosections were immunogold labeled with HMB50 (PAG 15, arrows) and αPmel-C (PAG10, arrowheads) and analyzed by IEM. After treatment with DAPT, note the αPmel-C labeling on endo-lysosomal structures and vesicles rather than at the limiting membrane of the PMEL luminal domain-positive compartment. Scale bar, 200 nm. **e.** Cells were analyzed

by conventional EM. Note the presence of the clathrin coats (black arrowheads) and MVEs (white arrow). Scale bar, 200 nm. **f.** Ultrathin cryosections were immunogold labeled for αPmel-C (PAG10 indicated by arrowheads). Note the presence of αPmel-C labeling at the limiting membrane of a clathrin coated MVE. Scale bar, 200 nm. **g.** MNT-1 cells were treated for 24 hrs with DMSO or 1 μM DAPT, and then lysed in buffer containing 1% Brij97. Lysates were immunoprecipitated with anti-MART-1 or anti-PMEL antibodies αPmel-C, HMB45, or HMB50, and immunoprecipitates or untreated lysate (Ext) were analyzed by immunoblot with an anti-ubiquitin antibody. Note the enrichment of ubiquitin signal in eluates from αPmel-C antibody immunoprecipitation after DAPT treatment.

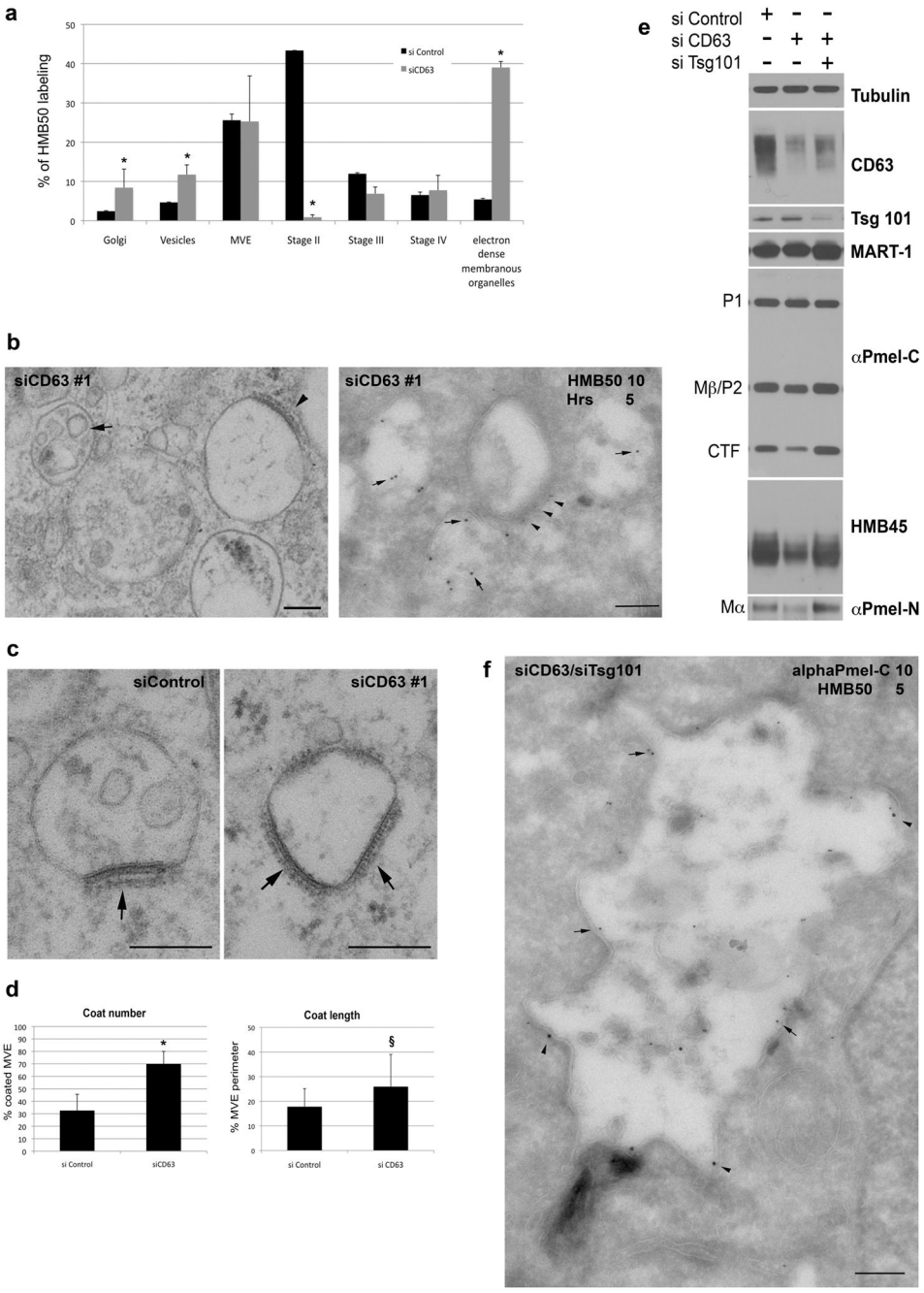

Figure 7. PMEL luminal domain is degraded in a ESCRT dependent manner in CD63 depleted cells

a. Quantification of immunogold labeling for PMEL luminal domain (HMB50) in different compartments on ultrathin cryosections of MNT-1 cells treated control or CD63#1 siRNA. Results are expressed as percentage (%) of total immunogold labeling in each compartments. **b, left panel:** MNT-1 cells treated with CD63#1 siRNA were analyzed by conventional EM. note the presence of MVEs (arrows) devoid of coats in the vicinity of coated vacuoles (arrowhead). Bar: 200nm. **Right panel:** Ultrathin cryosections of MNT-1 cells treated with CD63#1 siRNA were immunogold labeled with HMB50 (PAG 10, arrows) and Hrs (PAG5, arrowheads) and analyzed by IEM. Note the HMB50 labeling on endo-

lysosomal structures rather than in Hrs positive compartment. Scale bar, 200 nm. **c.** Representative micrographs of coated endosomes. Arrows indicate the characteristic bilayered coats that are expanded upon CD63 inactivation. Scale bar, 200 nm. **d.** Shown are the percentage (%) of coated endosomes relative to the total number of MVEs (left panel) and the mean length of the coat (right panel) measured on 50 profiles from each condition. *=P<0.01, §= P<0.05. **e.** Whole cell lysates of MNT-1 cells treated with control siRNA or CD63#1 siRNA alone or together with siRNA to Tsg101 were analyzed by western blot using antibodies to CD63, Tsg101, MART-1, or β-tubulin, or anti-PMEL antibodies αPmel-C, HMB45, or αPmel-N. Relevant bands are indicated. **f.** Ultrathin cryosections of MNT-1 cells treated with CD63 and Tsg101 siRNA were immunogold labeled with alphaPmel-C (PAG 10, arrowheads) and HMB50 (PAG5, arrows) and analyzed by IEM. Note that both labeling are broadly localized to the limiting membrane. Scale bar, 200 nm.